High levels of surface differential rotation on the young G0 dwarf HD 171488[⋆]

S. V. Jeffers[1,2]† and J.-F. Donati[2]

[1] *Sterrenkundig Instituut, Universiteit Utrecht, P.O. Box 80000, NL-3508 TA Utrecht, The Netherlands*
[2] *Laboratoire d'Astrophysique de Toulouse-Tarbes, Observatoire Midi-Pyrénées, 14, avenue Edouard Belin, F-31400 Toulouse, France*

ABSTRACT

We present high-resolution images of the young, rapidly rotating G0 dwarf HD 171488, using both Stokes I and Stokes V data. The observations were secured with the MuSiCoS spectropolarimeter at Telescope Bernard Lyot from 2005 May 31 to June 10. The photospheric surface brightness distributions show a strong and slightly decentred polar cap that dominates over weak high- and low-latitude spot features. The large-scale magnetic field topology shows a strong ring of anticlockwise azimuthal field with a latitudinal dependence on polarity and large regions of radial field with negative polarity at all latitudes. Using the good phase coverage of our data, we measure the differential rotation on HD 171488. The results indicate that the equator laps the pole every 12 days for brightness data and 13 days for magnetic data, which is the highest measurement of differential rotation obtained using Zeeman–Doppler imaging techniques.

Key words: line: profiles – stars: activity – stars: individual: HD 171488 – stars: magnetic fields – stars: rotation – stars: spots.

1 INTRODUCTION

Magnetic activity on the Sun and solar-like stars is generated by dynamo processes that essentially depend on differential rotation and convection. Differential rotation essentially results from the interplay of rotation and convection, which leads to a redistribution of heat and angular momentum in the stellar convective zone. The thermal and density profiles of the convective motions are responsible for producing a dependence of differential rotation on latitude and radius.

Helioseismological results confirm that on the Sun equatorial regions rotate faster than polar regions (Schou et al. 1998) and that radial shear is the strongest at the tacholine, which is located between the convection zone and the radiative core. For the case of the Sun, the $\alpha\Omega$ dynamo that amplifies the magnetic field is considered to be located in the tacholine. In this region, strong radial shear generates a toroidal (east–west) field from an initial poloidal field – the Ω effect. Toroidal field components are then converted to poloidal field through the action of rising plasma in the convection zone and the twisting of convective motions due to Coriolis forces (Steenbeck, Krause & Rädler 1966) – the α effect. The loop-like strands of magnetic flux are expelled into the convection zone as a consequence of a non-axisymmetric instability (Spruit & Van Ballegooijen 1982) and then rise to the surface. As the depth of the convective zone decreases, changes in the observed magnetic activity and dynamo processes are likely to take place, as we move from later to earlier spectral types.

Observations of star-spots on magnetically active stars can place constraints on the underlying magnetic amplification processes. Using tomographic techniques, such as (Zeeman–)Doppler imaging, differential rotation can be measured by tracing the movement of star-spots and magnetic features over several rotation cycles. This method includes a solar-like differential rotation law in the image-reconstruction process, where the rotation rate is allowed to vary smoothly with latitude, on an image gird (Donati et al. 2000). Other methods include matched-filter star-spot-tracking techniques, where individual star-spot-rotation rates are determined (Collier Cameron, Donati & Semel 2002). Using these techniques applied to unpolarized data, measurements of differential rotation have been obtained for HK Aqr (M 1.5V), LO Peg (K5V), AB Dor (K0V), PZ Tel (G9V), R58 (G2V) and LQ Lup (G2V). Barnes et al. (2005) show that there is a steady increase in the magnitude of differential rotation towards earlier spectral types, i.e. with increasing stellar mass, consistent with the theoretical predictions of Kitchatinov & Rüdiger (1999). Differential rotation measurements have also been determined using magnetic features for AB Dor and LQ Hya (Donati, Collier Cameron & Petit 2003b), where the degree of differential rotation is different when measured using brightness and

---

magnetic features. Donati et al. (2003b) conclude that this is the evidence of a non-solar dynamo that is distributed throughout the star's convective zone.

The motivation for this work is to understand how differential rotation is influenced by the depth of the star's outer convective zone, as we move to earlier spectral types. We also investigate if the difference between differential rotation measured with brightness and magnetic data increases or decreases with changing convective-zone depth. We extend the range of differential rotation measurements to hotter stars by observing the G0 dwarf HD 171488 (V889 Hercules). It is a magnetically active G0 dwarf that has been detected with the *ROSAT* EUV wide-field camera (Pounds et al. 1993) and the Extreme Ultraviolet Explorer, with count rates that indicate an active corona. Strassmeier et al. (2000) show that HD 171488 has strong Ca II H&K emission and a filled-in Hα absorption profile, both indicative of an active chromosphere, confirmed by Mulliss & Bopp (1994). HD 171488 is a rapid rotator, with a high vsini of between 33 and 44 km s^{-1} (Henry, Fekel & Hall 1995; Cutispoto et al. 2002) and an age ranging from 30 to 50 Myr (Strassmeier et al. 2003). It has previously been imaged using Doppler imaging by Strassmeier et al. (2003) and Zeeman–Doppler imaging by Marsden et al. (2006), where the resulting surface brightness images show a large polar cap and low latitude features. However, these analyses only use limited phase coverage, and Marsden et al. (2006) measure differential rotation, using brightness data only. We extend these previous works by reconstructing the surface brightness distributions and magnetic field topology, using well phase sampled spectropolarimetric data. The observations span several rotational periods, enabling us to measure differential rotation using both brightness and magnetic data.

2 OBSERVATIONS

HD 171488 was observed using the Telescope Bernard Lyot from 2005 May 31 to June 13, using the MuSiCoS echelle spectrograph (Baudrand & Bohm 1992, Donati et al. 1999) in polarimetric mode. The observations cover the wavelength range 450–660 nm, with a resolution of approximately 35 000.

2.1 Instrumental setup

To obtain circularly polarized Zeeman signatures from the stellar line profiles, the incoming stellar light is first passed through a quarter-wave plate, which converts circularly polarized light into linearly polarized light. The beam is then split, using a Savart plate, into two linearly polarized beams that are perpendicular and parallel to the Savart plate and fed, via optical fibres, to the spectrograph. Exposures of circularly polarized light comprise four subexposures, where the quarter-wave plate is rotated at angles ±45° in the sequence +45°, −45°, −45°, +45°. The polarization signal is therefore alternated in each output fibre removing spurious polarization signals. The four-subexposure sequence minimizes time-dependant effects, such as radial velocity variations, stellar variability and drifts in the spectrograph, as they become symmetric about the two middle subexposures.

2.2 Observational procedure

We were awarded 14 nights from 2005 May 31 to June 13. Favourable weather conditions allowed for seven full and three half nights of observations, as shown in Table 1. Exposure times for HD 171488 were 800 s for all spectra. Magnetic standards were also observed.

3 DATA PROCESSING

3.1 Data reduction

The raw echelle frames were reduced using ESPRIT, which is a dedicated package for the reduction of spectropolarimetric observations. Each stellar exposure contains information on two perpendicular states of circularly polarized light. They are extracted individually and in the same manner as for intensity spectra extraction, using the optimal-extraction routine of Marsh (1989). A detailed explanation of the extraction of polarized spectra is given by Donati et al. (1997).

3.2 Least-squares deconvolution

We use the technique of least-squares deconvolution (LSD) to compute average rotationally broadened profile for both the Stokes I and Stokes V data. The basic assumption of this technique is that the observed spectrum is equal to a convolution of a rotationally broadened mean profile and depth-weighted line pattern. When a weighted least-squares algorithm is used to compute the mean profile by optimizing the chi-squared fit to the data, LSD can extract rotation profiles from several thousand lines, simultaneously (Donati et al. 1997). LSD conserves the shape of the rotational profile, implying that any deviations in this profile can be interpreted as brightness inhomogeneities on the stellar surface. The list of spectral lines is obtained from the local thermodynamic equilibrium (LTE) model atmospheres of Kurucz (1993) for $T_{eff} = 5800$ K and

Table 1. Journal of observations. The rotational phases are computed using an ephemeris of HJD 245 3526.5 + 1.3371E, corresponding to the mid-point of the observations.

Date	JD 245 0000+	UT	Phase coverage	Exp time (s) per frame	No. of sequences (4 × 1 exp)	Ssignal-to-noise ratio (min/max; per exp)
2005 May 31	3522.4455	22:34:50/03:34:35	−3.032 to −2.884	800	5	47/100
2005 June 01	3523.3990	21:27:55/23:21:18	−2.319 to −2.133	800	2	
		23:54:16/03:41:14		800	4	44/120
2005 June 02	3524.5236	00:27:15/03:17:20	−1.478 to −1.397	800	3	65/110
2005 June 04	3526.4259	22:06:40/03:46:55	−0.055 to 0.114	800	6	75/110
2005 June 06	3528.4530	22:45:40/02:33:03	1.461 to 1.520	800	5	50/68
2005 June 07	3529.4186	21:56:08/03:37:20	2.183 to 2.353	800	6	55/95
2005 June 08	3530.3522	20:20:30/03:18:22	2.881 to 3.091	800	5	52/100
2005 June 09	3531.4239	22:03:44/02:47:20	3.683 to 3.793	800	5	62/100
2005 June 10	3532.3547	21:48:08/03:28:31	4.422 to 4.577	800	6	46/130

log $g = 4.5$. As shown by Jeffers et al. (2006a), there is no significant difference between spherical (PHOENIX) and plane-parallel model (ATLAS) atmospheres at F9V/G0V spectral type. For the LSD profile, a velocity step size of $4.6\,\mathrm{km\,s^{-1}}$ was used to match the resolution of the observations.

Using 1997 lines, the average multiplex gain is approximately 17 for Stokes I and approximately 25 for Stokes V. As discussed by Donati et al. (1997), the application of LSD to Stokes I is less efficient than to Stokes V. This is due to the dominant noise in the unpolarized profiles being caused by the blending of neighbouring spectral lines that are inaccurately modelled, whereas the dominant noise in the polarized spectra is photon noise.

3.3 Telluric lines

We use telluric lines to account for small-scale variations in the spectrograph during the night, as they are only present in the Earth's atmosphere and are therefore at zero radial velocity. The LSD profile of the Stokes I data is shifted to match the LSD profile of the telluric lines contained within the spectrum. This procedure has previously been applied by Donati et al. (2003a) and Jeffers, Donati & Collier Cameron (2007) to obtain accurate radial velocity measurements of AB Dor.

4 SURFACE IMAGES

The stellar surface brightness and magnetic images are reconstructed using the maximum entropy code of Brown et al. (1991) and Donati & Brown (1997) from the rotationally modulated Stokes I and V profiles. As image reconstruction is an ill-posed problem, the code incorporates the Skilling & Bryan (1984) maximum-entropy algorithm, which results in an image with the lowest amount of information.

4.1 Stellar parameters

The system parameters of HD 171488 – temperature, rotational velocity and radial velocity – were determined using chi-square minimization, where a parabolic function is fitted to the chi-square values to determine the minimum. Parameters taken from the literature include: the rotational period of 1.3371 d, from the photometric observations of Strassmeier et al. (2003), and limb darkening coefficient 0.684 ($T = 5750\,\mathrm{K}$ and log $g = 4.5$), from the tabulated models of Diaz-Cordoves, Claret & Gimenez (1995).

The temperature is determined by using PHOENIX model-atmosphere spectra. Model atmospheres, ranging in temperature from 5300 to 6200 K in 100 K steps, were fitted to the spectra of HD 171488, using chi-square minimization. The minimum chi-square value (as shown in Fig. 1) corresponds to a temperature of $5808 \pm 43\,\mathrm{K}$, in good agreement with the value of 5830 K, used by Strassmeier et al. (2003).

The radial velocity and the projected rotational velocity, vsini, of HD 171488 were determined by reconstructing several surface brightness images, using incremental input values. Images to determine the radial-velocity value were reconstructed with $0.1\,\mathrm{km\,s^{-1}}$ as the incremental value. The value for the vsini was also obtained by fitting a parabolic function to the chi-square values of the surface images, reconstructed with incrementing values of $0.5\,\mathrm{km\,s^{-1}}$. This method excludes the possibility that the result could be biased by the presence of star-spots and, in particular, by shallow profiles caused by a large polar spot. As shown in Fig. 2, the vsini of HD 171488 is
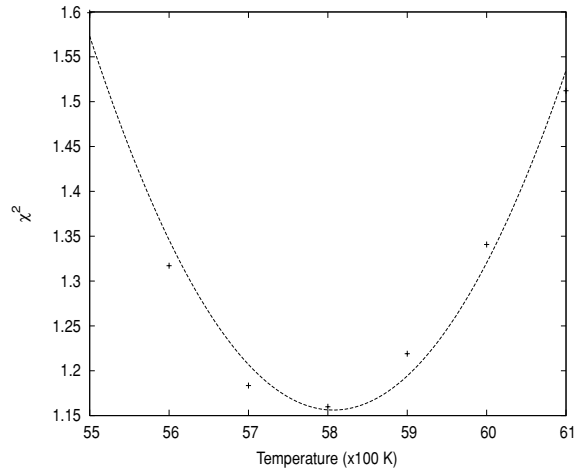

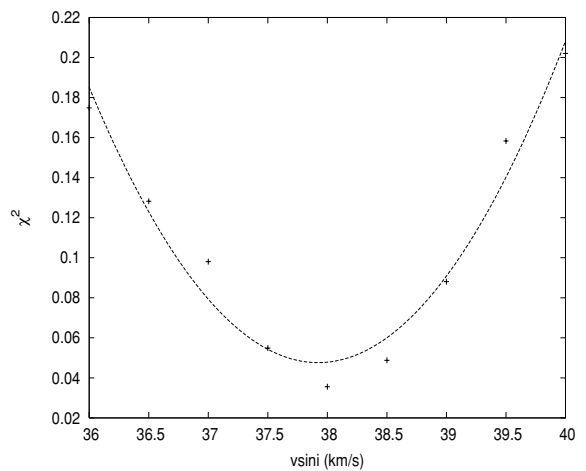**Figure 1.** The temperature of HD 171488 as determined by fitting PHOENIX model-atmosphere spectra.

Figure 2. The vsini of HD 171488 as determined by chi-square minimization.

$38.0 \pm 0.5\,\mathrm{km\,s^{-1}}$, which is comparable to value found by Marsden et al. (2006) of $37.5 \pm 0.05\,\mathrm{km\,s^{-1}}$.

The inclination was determined using the rotational period from Strassmeier et al. (2003) and the radius from Marsden et al. (2006) that were determined from the absolute bolometric magnitude of HD 171488. This results in an inclination of 60°. The fundamental parameters of HD 171488 are summarized in Table 2.

4.2 Surface brightness image

The brightness images are reconstructed using the two-component model of Collier Cameron (1992), where all spots have the same temperature and any contributions from the penumbrae are neglected. Each point on the stellar surface is quantified by 'spot occupancy' that ranges from 0 for no spots to 1 for maximum spottedness. A synthetic Gaussian profile is used as the average intrinsic line profile, where the full width at half-maximum (FWHM) is set to be equal to the FWHM of the LSD profile of the slowly rotating standard star HD 168009. The Gaussian template profile is scaled with the ratio 1:5 to represent the spotted and quiet photosphere, respectively (Strassmeier et al. 2003).

Table 2. Summary of the fundamental parameters of HD 171488 used in this paper. The rotational period of Strassmeier et al. (2003) is used as it is derived from photometric data. The radius of Marsden et al. (2006) is used as it is derived from the absolute bolometric magnitude.

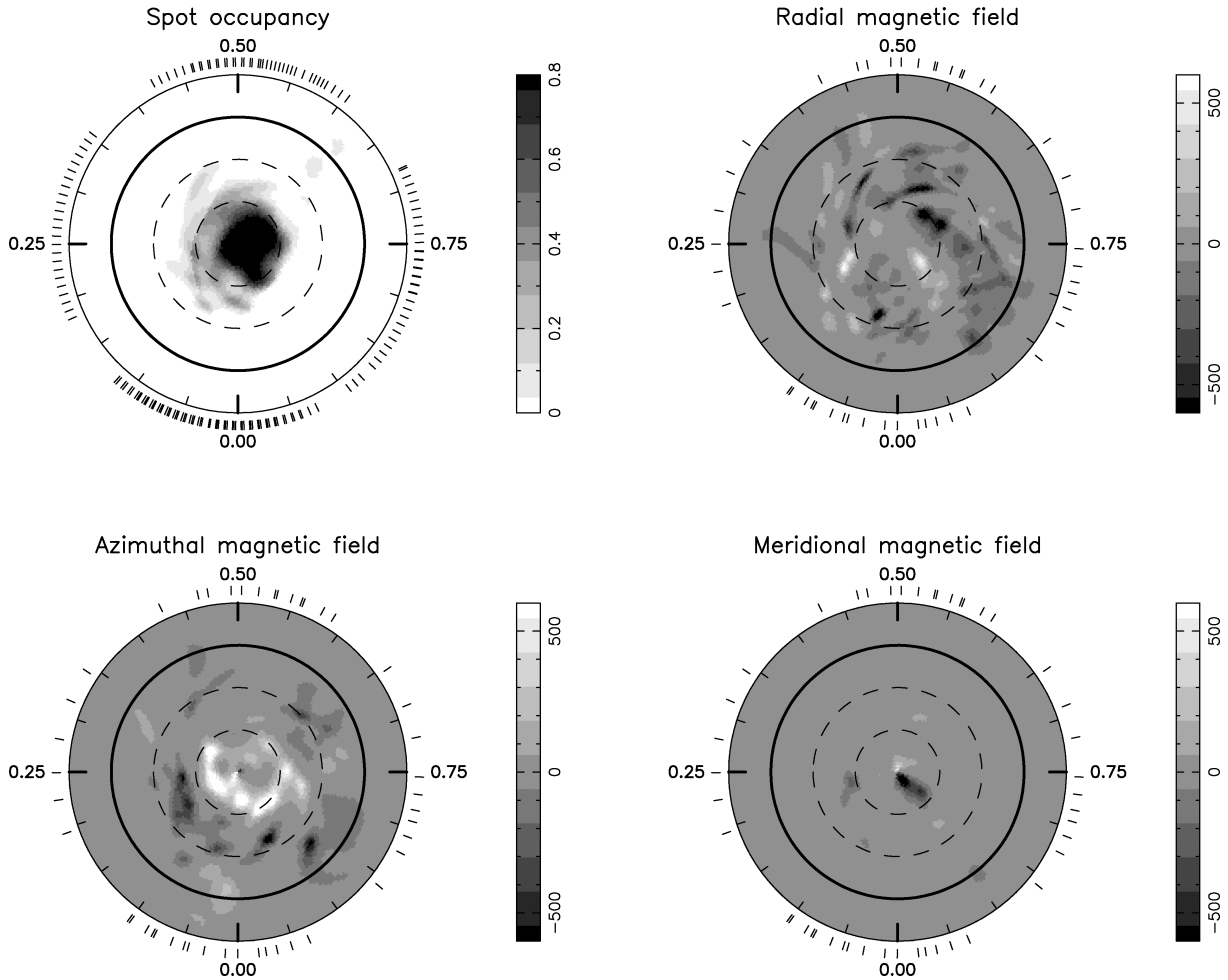| Parameter	Value	Source
Inclination	$60° \pm 10°$	This work
Vsini	$38.0 \pm 0.5 \, \mathrm{km \, s^{-1}}$	This work
Radial velocity	$-22.90 \pm 0.1 \, \mathrm{km \, s^{-1}}$	This work
Photospheric temperature	5808 K	This work
Spot temperature	4200 K	Strassmeier et al. and Marsden et al.
Rotation period	1.3371 ± 0.0002 d	Strassmeier et al.
Radius	$1.15 \pm 0.08 \, \mathrm{R_\odot}$	Marsden et al.

Figure 3. Maximum entropy brightness (top left-hand panel) and magnetic maps of HD 171488 for 2005 May 31–June 10. These images are flattened polar projections extending down to a latitude of $-30°$, where the bold line depicts the equator and the dashed lines are at $30°$ intervals. The radial ticks surrounding each image indicate the rotational phase of individual Stokes I and V observations. The scale of the magnetic field strengths are in Gauss, where positive field values correspond to magnetic vectors directed outward, anticlockwise and poleward, respectively, for radial, azimuthal and meridional field components. The images shown here include the values for differential rotation measured in Section 5 to avoid smearing of spots over the long phase coverage of our data set.

The reconstructed surface brightness image of Stokes I data of HD 171488 is shown in Fig. 3, with the maximum entropy fits to the profiles shown in Fig. 4. As the phase coverage is approximately 0.2 per night, we reconstruct an image, using the full data set. The surface image-reconstruction code also incorporates the stellar differential rotation, which is determined in Section 5, and accounts for surface evolution of star-spots over the 11-d time-span of the data set.

The reconstructed spot features are more reliable than those shown in the previous analyses of Marsden et al. (2006) and Strassmeier et al. (2003), due to the excellent phase coverage of our data set. The most notable feature of the reconstructed images is the strong and slightly decentred polar cap that extends to $60°$ in latitude and which dominates over weak, high-latitude spot features. Despite a few small gaps in the phase coverage, the reconstructed features at these phases for polar and high latitudes are reliable, with
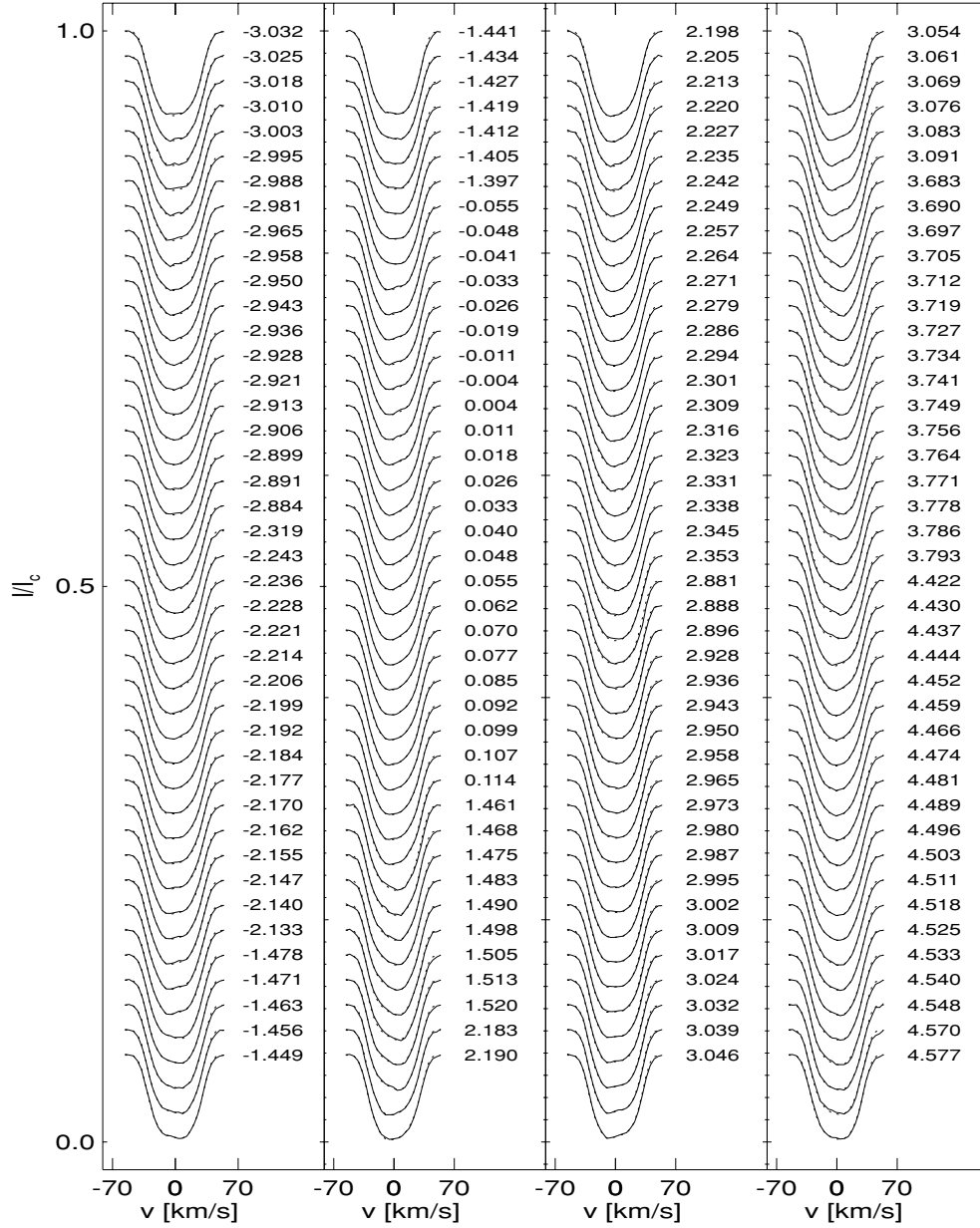
Figure 4. Maximum entropy fits (dashed line) to the Stokes I LSD profiles (solid line). The rotational phase is located to the right of each profile.

no north–south smearing, as the axial inclination of HD 171488 is 60°. The reconstructed surface brightness image is in broad agreement with the results of Marsden et al. (2006), though their poor phase coverage results in a more speckled polar cap, and the image of Strassmeier et al. (2003), where the polar cap is more compact but which also extends to ≈60° at phase ≈0.75. The reconstructed image of this analysis does not show any reliable low-latitude spots. However, the surface brightness image of Marsden et al. (2006) shows two small surface features at a latitude of 30° at phase 0.75 and 0.85, though the second feature is not reliable, given that there are no observations at this rotational phase. Likewise, the image of Strassmeier et al. (2003) shows several low-latitude spots, but they conclude that these are too weak to be significant and that these are biased by uneven phase coverage.

The fractional spot occupancy as a function of latitude is determined from

$$F(l) = \frac{S(l)\cos(l)\mathrm{d}l}{2},$$ (1)

where $F(l)$ is the fractional spottedness at latitude l and $S(l)$ is the average spot occupancy at latitude l. The resulting plot, Fig. 5, shows that star-spot coverage is predominantly at polar and high latitudes. The fractional spot occupancy as a function of longitude is shown in Fig. 6, which clearly shows that there are no active longitudes on HD 171488.

4.3 Surface magnetic field topology

The reconstruction of magnetic images assumes weak magnetic fields and a constant Gaussian profile over the stellar surface. The three components of the magnetic field vector are reconstructed, i.e. radial, meridional and azimuthal components. These are weighted
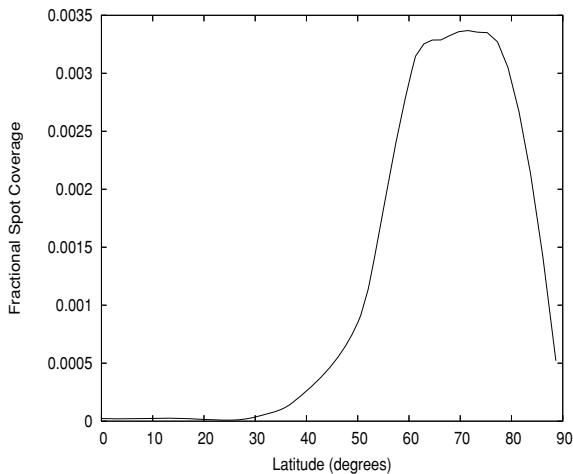
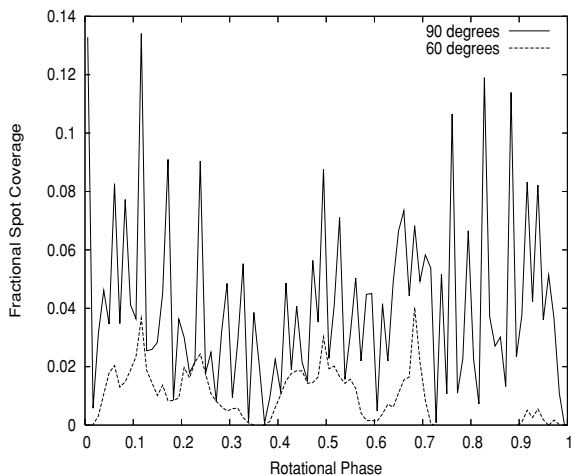**Figure 5.** Fractional spot coverage per latitude bin, integrated over longitude.

Figure 6. Fractional spot coverage per longitude bin integrated over latitude 0°–90° and 0°–60°, showing no evidence for active longitudes on HD 171488.

by potential surface inhomogeneities in brightness, local magnetic field occupancy and the central depth of the intrinsic profile.

The reconstructed large-scale magnetic field topology of HD 171488 from Stokes V data is shown in Fig. 3, with the fits to the Stokes V profiles shown in Fig. 7. The quadratic magnetic flux, which is defined as the product of the local field modulus and the local surface area, is calculated to be 68 G. The main difference between the reconstructed magnetic and brightness images is the lack of polar features in the magnetic maps, which could be caused by the reduced flux, and hence magnetic field signatures, emanating from the polar regions of HD 171488.

The most notable feature of azimuthal field topology of HD 171488 is the ring of anticlockwise field surrounding the rotational pole, whereas at low latitudes, an anticlockwise field dominates, with small localized regions of clockwise field also present. The ring of anticlockwise azimuthal field is also present in the images of Marsden et al. (2006) but not as strong or consistent as shown in our images. The reconstructed radial magnetic field topology is dominated by negative-polarity field that extends to low and equatorial latitudes. Smaller positive magnetic field regions are

also present at all latitudes. The meridional magnetic field maps show only weak-field structures. This could be due to our imaging code not being very sensitive to low latitude meridional fields for stars with high inclination angles, as discussed by Donati & Brown (1997). The majority of magnetic energy is stored in the azimuthal component, 55 per cent, whereas the radial component contains 38 per cent and the meridional component, 6 per cent.

5 DIFFERENTIAL ROTATION

The image reconstruction process also incorporates a model of the stellar differential rotation, where the rotation rate Ω depends on latitude, according to the simplified solar-like differential rotation law,

$$\Omega(\theta) = \Omega_{eq} - \delta\Omega \cos^2 \theta, \tag{2}$$

where $\Omega(\theta)$ is the rotation rate at colatitude θ, Ω_{eq} is the equatorial rotation rate and $\delta\Omega$ is the difference between polar and equatorial rotation rates (Petit, Donati & Collier Cameron 2002). A two-dimensional grid of values for $\Omega_{eq}, \delta\Omega$ is then computed, where, for each permutation of values, the image-reconstruction code is driven until it reaches a fixed value of spot-filling factor for Stokes I data and the quadratic magnetic flux for Stokes V data. The resulting chi-square values for each model are then plotted as a landscape, where the best-fitting model corresponds to the minimum in the chi-square landscape.

5.1 Stokes I data

The imaging code was converged to a spot-filling factor of 7 per cent, obtained when reconstructing the surface brightness image, and was used to compute a grid of Ω–dΩ models. The resulting chi-square landscape is shown in Fig. 8 and fitting the paraboloid resulted in the following parameters: derived equatorial rotation rate with 68 per cent (1σ) confidence interval, $\Omega_{eq} = 4.93 \pm 0.05$ rad d^{-1}; difference in pole-equator rotation rate d$\Omega = 0.52 \pm 0.04$ rad d^{-1} and total number of data points, $n = 4200$. These values translate to a beat period of 12 ± 1 d. The change in the LSD profile due to the effects of differential rotation is shown in Fig. 9, where the Stokes I LSD profile is shown for the same rotational phase but separated by several rotations.

5.2 Stokes V data

Differential rotation for Stokes V data was determined using spherical harmonics inversion. We use this method to avoid the result being biased by the emergence of new magnetic features over the time-span of the observations, which can happen when the sheared image method is used. Further details of this method can be found in Donati et al. (2006a,b). The resulting chi-square landscape is shown in Fig. 10 and fitting the paraboloid resulted in the following parameters: $\Omega_{eq} = 4.85 \pm 0.05$ rad d^{-1}; d$\Omega = 0.47 \pm 0.04$ rad d^{-1} and $n = 1125$. These values translate to a beat period of 13 ± 2 d. The effect of differential rotation on the Stokes V LSD profile is shown in Fig. 11, where three profiles are shown at the same rotational phase but separated by three stellar rotations.
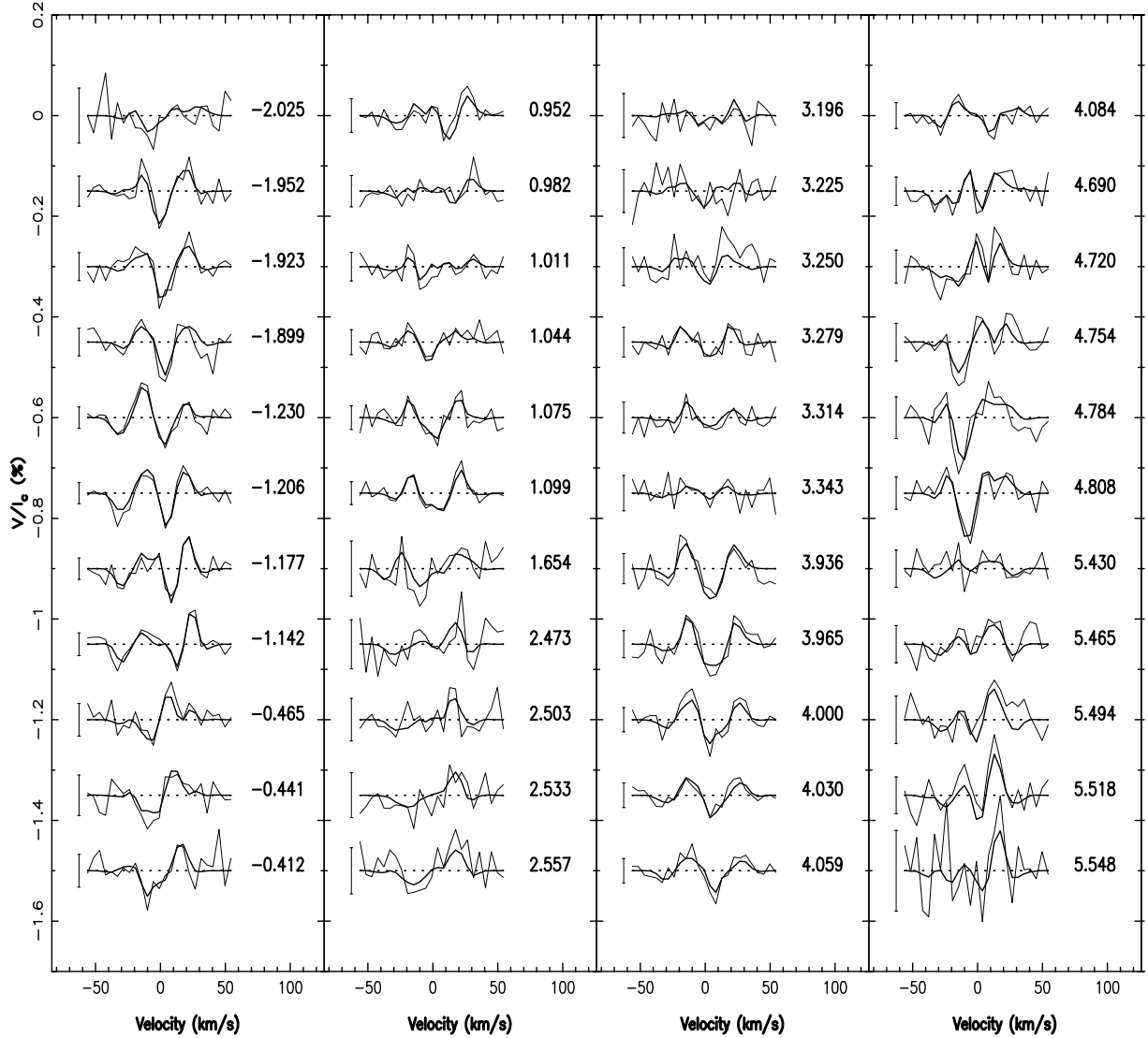
Figure 7. Maximum entropy fits (thick solid line) to the Stokes V LSD profiles (narrow solid line), where the error bars and rotational phases are, respectively, located to the left- and right-hand side of each profile.

6 DISCUSSION

6.1 Surface brightness distributions

The reconstructed surface brightness distribution of HD 171488 (Fig. 3, top left-hand image) shows a strong decentred polar cap that dominates over weak high-latitude spot features. In general, the distribution of spots is in agreement with the previous surface images of Marsden et al. (2006) and Strassmeier et al. (2003), which show a large polar spot and several possible low-latitude features. However, the detailed reconstruction of this analysis is more reliable due to the excellent phase coverage of our data set. By splitting the data set into two parts, comprising the first and the last four nights, respectively, and reconstructing surface brightness images for each set, we show that at overlapping phases, there is no evidence for the emergence of new star-spots over the time-span of our data set.

Direct evidence for the presence of a polar cap has been shown by Jeffers et al. (2005, 2006b) using data from the *Hubble Space Telescope* (*HST*) of the RS CVn binary SV Cam. In these analyses, it is shown that when fitting model-atmosphere spectra to the spec-

trophotometric observations, there is a flux deficit that can only be accounted for by the presence of many subresolution spots and a polar cap. The presence of many subresolution spots on active stars has also been shown by TiO-band analysis (O'Neal, Neff & Saar 1998). This does not imply that the Doppler images reconstructed in this analysis are inaccurate, but that they show the locations of the main-spot groupings on the surface of HD 171488.

HD 171488 is a young, rapidly rotating star, just approaching the main sequence. Other stars of similar age and spectral type that have been Doppler imaged include R58 ($B - V = 0.61$, 35 Myr, $p = 0.57$ d; Marsden et al. 2005), H II 314 (G1–2V, 100 Myr, $p = 1.47$ d; Rice & Strassmeier 2001), LQ Lup (G2V, 25 Myr, $p = 0.31$ d; Donati et al. 2000), He 699 (G1–2V, 50 Myr, $p = 0.49$ d, Barnes et al. 2001; Jeffers, Barnes & Collier Cameron 2002). In general, all of the reconstructed images of these stars show predominantly polar and high-latitude structure, with the images of R58, H II 314 and LQ Lup also showing low latitude features. Similar spot distributions, but with more low-latitude features, are also found on lower mass stars such as the K0 V dwarf AB Dor by Donati et al. (2003a) and Jeffers et al. (2007). However, images of the M dwarfs HK Aqr and
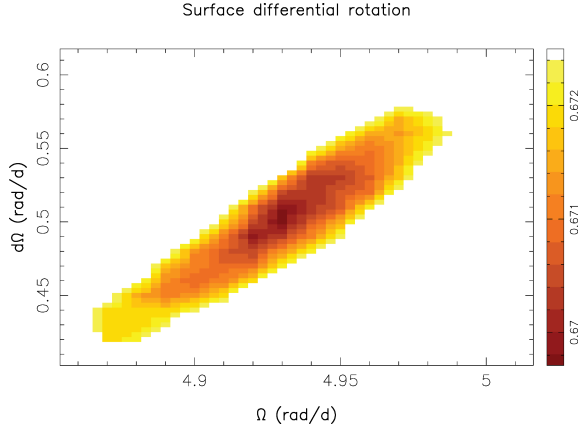
Figure 8. Reduced chi-square maps in Ω_{eq}–dΩ plane for HD 171488. Each permutation in Ω_{eq}–dΩ was converged to a fixed spot coverage of 0.0705. The outer edge of the ellipsoid corresponds to the 1.5σ confidence ellipse (taking each parameter separately) on the differential rotation parameter plane.

Figure 10. Same as for Stokes I data but using Stokes V converged to a fixed value of 68 G. The outer edge of the ellipsoid corresponds to the 1σ confidence ellipse.

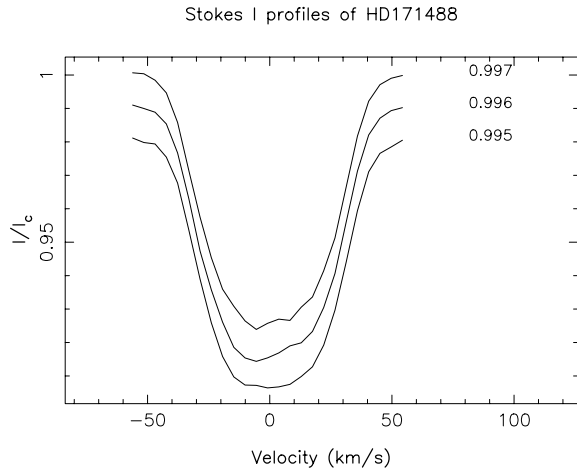**Figure 9.** Stokes I LSD profiles of HD 171488 at the same rotational phase but separated, respectively, by two and three stellar rotations.

Figure 11. Stokes V LSD profiles of HD 171488 at the same rotational phase with a separation of three stellar rotations between each profile.

EY Dra, reconstructed by Barnes & Collier Cameron (2001), show spots at all latitudes but without a polar cap.

6.2 Magnetic field topology

The reconstructed large-scale magnetic field topology, comprising radial, azimuthal and meridional magnetic field components, is shown in Fig. 3. The azimuthal field topology (Fig. 3, bottom left panel) is dominated by a strong ring of positive (anticlockwise) azimuthal field that surrounds the rotational axis. Unlike the reconstructions of the radial magnetic field topology, there is an obvious latitudinal dependence. The strong ring of positive azimuthal field dominates at latitudes greater than $\approx 55°$, with negative polarities dominating at latitudes $\approx 30°$ to $\approx 55°$ and with additional small isolated regions of positive field at latitudes $\leq 30°$. The reconstructed azimuthal field topologies of HD 171488 by Marsden et al. (2006) show a similar azimuthal field ring structure but in the form of a large field concentration at phase 0.3, a weaker field concentration from phase 0.95 to 0.3, and a weak isolated concentration of magnetic flux at phase 0.75.
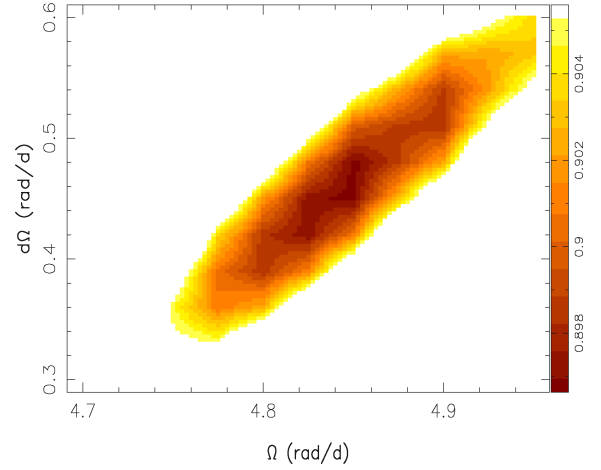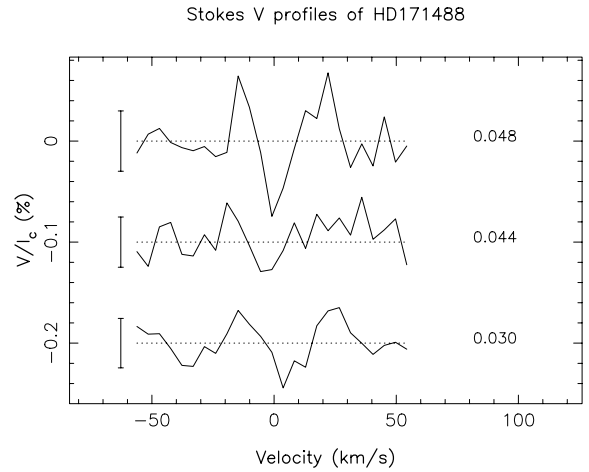
A polar ring of azimuthal field and latitudinal banding has also been observed on AB Dor (Donati et al. 2003a), where the average azimuthal field topology, over the 10 yearly spaced epochs of the data sets from 1995 to 2004, shows a persistent ring of clockwise field at the pole. The latitudinal polarity pattern has also been consistently observed on LQ Hya (K0V) and HR 1099 (K1IV). As discussed by Donati et al. (2003a), the azimuthal component is interpreted to be representative of the toroidal component of the large-scale dynamo field. Due to convective motions, such large amounts of horizontal field structure could not preserve their structure at the stellar photosphere if they were produced in the thin overshoot layer at the base of the convective zone (Donati et al. 2003a). This could imply that there is a non-solar-type dynamo process, generating magnetic fields in the subsurface regions of the star (Dikpati et al. 2002), with strong radial rotation (Corbard & Thompson 2002) or distributed throughout the convective zone (Lanza, Rodonò & Rosner 1998).

The radial magnetic topology (Fig. 3, top right panel) is predominantly in the form of large negative-field concentrations that extend to equatorial latitudes, with small amounts of positive field distributed at all latitudes. There is no apparent latitude dependence,

which is consistent with the radial magnetic field topologies, reconstructed for other late-type stars such as AB Dor (K1V) and LQ Hya (K0V). The radial field topologies reconstructed of HD 171488 by Marsden et al. (2006), show mixed polarity structures, where the negative field is slightly more dominant. As with the magnetic field topologies reconstructed in this analysis, Marsden et al. (2006) show no latitude dependence of polarity, but their images seem to indicate a dependence on longitude, which is not shown in our images. It should be noted that although the signal-to-noise ratio and resolution of their observations are higher than ours, their magnetic field distributions are reconstructed with only seven phase points. The limited phase coverage of this data set is likely to be the reason for the reconstructed longitudinal dependence. As discussed by Donati et al. (2003a), the radial component is interpreted to be representative of the poloidal component of the large-scale dynamo field.

It is shown that the majority of magnetic energy is stored in the azimuthal component (55 per cent), whereas the radial component contains 38 per cent and the meridional component 6 per cent. These fractional distributions are similar to that determined for HD 171488 by Marsden et al. (2006), AB Dor and LQ Hya (Donati et al. 2003a).

The latitudinal distribution of toroidal and poloidal magnetic field components is a further indication of the dynamo operating in these stars. As discussed above, the latitudinal distribution is much more complex than observed on the Sun, which would indicate a more complex dynamo operating in such young active stars as HD 171488. Given the similarity in spectral type, the complex field structures observed on HD 171488 could indicate that the nature of the dynamo changes as the star evolves.

Further work, using these observations, will be to extrapolate the magnetic field to understand how the magnetic field influences the rotational evolution of the star through magnetic braking.

6.3 Differential rotation

The surface differential rotation of HD 171488 is the highest ever measured using Stokes I or Stokes V data and the (Zeeman–) Doppler imaging technique. Barnes et al. (2005) have investigated differential rotation as a function of spectral type. The results show that there is a steady increase in the magnitude of differential rotation, from almost solidly rotating M-dwarfs towards earlier spectral types, i.e. with increasing stellar mass, where several early G-dwarfs show differential rotation, approximately three times greater than solar values. HD 171488 does not lie on the power-law fit of Barnes et al. (2005) with our value of differential rotation, which is almost nine and 10 times greater than solar for the brightness and magnetic data. In contrast, differential rotation measurements for other early G-dwarfs, LQ Lup (Donati et al. 2000) and R58 (Marsden et al. 2005), are approximately half of what we have measured for HD 171488 [LQ Lup: $\Omega_{eq} = 20.28 \pm 0.01$ rad d^{-1}, d$\Omega = 0.12 \pm 0.02$ rad d^{-1}; R58 (2000 Jan/2003 Mar): $\Omega_{eq} = (11.139 \pm 0.008)/(11.190 \pm 0.006)$ rad d^{-1}, d$\Omega = (0.025 \pm 0.015)/(0.138 \pm 0.011)$ rad d^{-1}]. Previous measurements of the differential rotation of HD 171488 by Marsden et al. (2006) are comparable within errors, even though their observations were taken nine months before our data set. The implication for understanding how differential rotation depends on fundamental stellar parameters is not clear, as LQ Lup, R58 and HD 171488, all have similar spectral type, mass and radius. The difference in their rotational periods has been shown by Barnes et al. (2005) to be a negligible parameter. High levels of differential rotation (<0.5 rad d^{-1}) have also been measured on F dwarfs by Reiners (2006) and Reiners & Schmitt (2003) using line

profile analysis. Their results would support our measurement of high differential rotation on HD 171488.

Little is currently known about the driving mechanisms of differential rotation. For example, Brun & Toomre (2002) claim that Reynold's stresses are the main driver for grossly reproducing the radial and azimuthal patter of angular rotation on the Sun, whereas Rüdiger & Küker (2002) claim that thermal effects dominate in rapidly rotating stars. Other theoretical models (Kitchatinov & Rüdiger 1999; Küker & Rüdiger 2005) that model internal fluid motions show that surface differential rotation should vary as a function of increasing stellar mass, for spectral types K5 to G2, but the magnitude of increase in differential rotation is not as strong as observations indicate. However, it should be considered that the observed stars have higher rotational velocities, and that the models are in reasonable agreement with the unweighted fit of Barnes et al. (2005).

Another important result is that the differential rotation measurement obtained from Stokes V data is approximately the same as that derived from the Stokes I data. Other measurements of differential rotation, using both brightness and magnetic data, have been made for AB Dor (Donati et al. 2003b), where there is a large variation between the two data sets. As discussed in Donati et al. (2003b), this effect is not an artefact of the imaging process, especially when the phase coverage is well sampled, and indicates that magnetic regions are not anchored at the same depth in the convective zone and therefore do not experience the same shear. The marginal difference in the differential rotation measurements for Stokes I and V data for HD 171488 provides further evidence for the existence of a non-solar-type dynamo, as HD 171488 has a much thinner convective zone than AB Dor.

Helioseismological results of acoustic wave propagation through the Sun show differential rotation throughout the outer convective zone, with the strongest shear being at the tacholine. In current models of magnetic field amplification in the Sun, it is in the tacholine that the Ω effect converts poloidal to toroidal field through strong radial shear. With the thin convective zone of HD 171488, it could be possible that we are seeing more effects of the strong radial shear of the tacholine. It could also be possible that there is a stronger dependence on rotational velocity compared with a K dwarf, due to the moment of inertia of the convection zone being smaller.

We have been awarded further time, using NARVAL at Telescope Bernard Lyot, to determine if there is a temporal evolution of differential rotation on HD 171488. The results will be presented in a forthcoming paper.

REFERENCES

Barnes J. R., Collier Cameron A., 2001, MNRAS, 326, 950
Barnes J. R., Collier Cameron A., James D. J., Steeghs D., 2001, MNRAS, 326, 1057
Barnes J. R., Cameron A. C., Donati J.-F., James D. J., Marsden S. C., Petit P., 2005, MNRAS, 357, L1
Baudrand J., Bohm T., 1992, A&A, 259, 711
Brown S. F., Donati J.-F., Rees D. E., Semel M., 1991, A&A, 250, 463
Brun A. S., Toomre J., 2002, ApJ, 570, 865

Collier Cameron A., 1992, in Byrne P. B., Mullan D. J., eds, Surface Inhomogeneities on Late-type Stars (Invited Review) Modelling Stellar Photospheric Spots Using Spectroscopy. Springer-Verlag, Berlin, p. 33

Collier Cameron A., Donati J.-F., Semel M., 2002, MNRAS, 330, 699

Corbard T., Thompson M. J., 2002, Sol. Phys., 205, 211

Cutispoto G., Pastori L., Pasquini L., de Medeiros J. R., Tagliaferri G., Andersen J., 2002, A&A, 384, 491

Diaz-Cordoves J., Claret A., Gimenez A., 1995, A&AS, 110, 329

Dikpati M., Corbard T., Thompson M. J., Gilman P. A., 2002, ApJ, 575, L41

Donati J.-F., Brown S. F., 1997, A&A, 326, 1135

Donati J.-F., Semel M., Carter B., Rees D. E., Collier Cameron A., 1997, MNRAS, 291, 658

Donati J.-F., Catala C., Wade G. A., Gallou G., Delaigue G., Rabou P., 1999, A&A, 134, 149

Donati J.-F., Mengel M., Carter B., Marsden S., Collier Cameron A., Wichmann R., 2000, MNRAS, 316, 699

Donati J.-F. et al., 2003a, MNRAS, 345, 1145

Donati J.-F., Collier Cameron A., Petit P., 2003b, MNRAS, 345, 1187

Donati J.-F., Forveille T., Cameron A. C., Barnes J. R., Delfosse X., Jardine M. M., Valenti J. A., 2006a, Sci., 311, 633

Donati J.-F. et al., 2006b, MNRAS, 370, 629

Henry G. W., Fekel F. C., Hall D. S., 1995, AJ, 110, 2926

Jeffers S. V., Barnes J. R., Collier Cameron A., 2002, MNRAS, 331, 666

Jeffers S. V., Cameron A. C., Barnes J. R., Aufdenberg J. P., Hussain G. A. J., 2005, ApJ, 621, 425

Jeffers S. V., Aufdenberg J. P., Hussain G. A. J., Cameron A. C., Holzwarth V. R., 2006a, MNRAS, 367, 1308

Jeffers S. V., Barnes J. R., Cameron A. C., Donati J.-F., 2006b, MNRAS, 366, 667

Jeffers S. V., Donati J.-F., Collier Cameron A., 2007, MNRAS, 375, 567

Kitchatinov L. L., Rüdiger G., 1999, A&A, 344, 911

Kurucz R. L., 1993, CDROM 13 (ATLAS9 atmospheric models) and 18 (ATLAS9 and SYNTHE routines, spectral line data base). Cambridge, MA

Küker M., Rüdiger G., 2005, A&A, 433, 1023

Lanza A. F., Rodono M., Rosner R., 1998, MNRAS, 296, 893

Marsden S. C., Waite I. A., Carter B. D., Donati J.-F., 2005, MNRAS, 359, 711

Marsden S. C., Donati J.-F., Semel M., Petit P., Carter B. D., 2006, MNRAS, 370, 468

Marsh T. R., 1989, PASP, 101, 1032

Mulliss C. L., Bopp B. W., 1994, PASP, 106, 822

O'Neal D., Neff J., Saar S., 1998, ApJ, 507, 919

Petit P., Donati J.-F., Collier Cameron A., 2002, MNRAS, 334, 374

Pounds K. A. et al., 1993, MNRAS, 260, 77

Reiners A., 2006, A&A, 446, 267

Reiners A., Schmitt J. H. M. M., 2003, A&A, 412, 813

Rice J. B., Strassmeier K. G., 2001, A&A, 377, 264

Rüdiger G., Küker M., 2002, A&A, 385, 308

Schou J. et al., 1998, ApJ, 505, 390

Skilling J., Bryan R. K., 1984, MNRAS, 211, 111

Spruit H. C., Van Ballegooijen A. A., 1982, A&A, 106, 58

Steenbeck M., Krause F., Rädler K. H., 1966, Zeitschrift Naturforsch. Teil A, 21, 369

Strassmeier K., Washuettl A., Granzer T., Scheck M., Weber M., 2000, A&AS, 142, 275

Strassmeier K. G., Pichler T., Weber M., Granzer T., 2003, A&A, 411, 595

This paper has been typeset from a TEX/LATEX file prepared by the author.